Velocity estimation by image focusing analysis

*Biondo Biondi *, Stanford University.*

SUMMARY

Migration velocity can be estimated from seismic data by analyzing focusing and defocusing of residual-migrated images. The accuracy of these velocity estimates is limited by the inherent ambiguity between velocity and reflector curvature. However, velocity resolution improves when reflectors with different curvatures are present. Image focusing is measured by evaluating coherency across structural dips, in addition to coherency across aperture/azimuth angles. The inherent ambiguity between velocity and reflector curvature is directly tackled by introducing a curvature correction into the computation of the semblance functional that estimates image coherency. The resulting velocity estimator provides velocity estimates that are: 1) unbiased by reflector curvature, and 2) consistent with the velocity information that we routinely obtain by measuring coherency over aperture/azimuth angles. The application of the proposed method to zero-offset field data recorded in New York Harbor yields a velocity function that is consistent with available geologic information and clearly improves the focusing of the reflectors.

INTRODUCTION

The effect of migration velocity on the focusing and unfocusing of seismic images is obvious when observing migrated seismic images obtained with different migration velocities. Quantitative measures of image focusing can extract from the data valuable information for velocity estimation. This information is particularly abundant in areas where reflectors have strong curvature or are discontinuous, such as in heavily faulted and folded geology, or in the presence of buried channels, uncomformities, or rough salt/sediment interfaces. However, it is difficult to define objective quantitative criteria to measure image focusing. Criteria that have been previously proposed to measure image focusing, such as maximization of the power of the stack or minimization of image entropy (Harlan et al., 1984; De Vries and Berkhout, 1984; Stinson et al., 2005; Fomel et al., 2007), would be biased when there are reflectors with high-curvature but not infinite curvature in the subsurface. Positive curvature reflectors (e.g. anticlines) cause velocity to be overestimated, whereas negative curvature reflectors (e.g. synclines) cause velocity to be overestimated. Consequently, current practical methods for exploiting image-focusing information are based on subjective interpretation criteria instead of quantitative measurements (Sava et al., 2005; Wang et al., 2006).

If we could extract quantitative focusing-velocity information reliably from migrated images, it could supplement the velocity information that we routinely extract by analyzing residual moveout along offsets (after common-offset migration) or aperture-angles (after angle-domain migration) axes. In practice, velocity analysis based on image focusing is unlikely to replace conventional velocity analysis, but only to supplement it. Therefore, a method that measures image focusing should provide velocity estimates that are consistent with conventional methods. This abstract aims to overcome the shortcomings of current methods used to measure image focusing. It presents a new method that has two important characteristics: 1) the velocity information it provides is consistent with the velocity information obtained by analyzing the coherence of migrated images along the reflection-aperture angle axes, and 2) it explicitly takes into account the relation between reflector curvature and velocity.

IMAGE-FOCUSING SEMBLANCE

The main goal of the image-focusing semblance is to extend the conventional semblance evaluation by measuring image coherency also along the the structural-dip axes. First, I define a semblance measure that is independent from reflector curvature, but that implicitly assumes the presence of reflectors with infinite curvature; that is, point diffractors. To prevent reflector curvature from biasing the velocity estimates, I then include the curvature information in the definition of the image-focusing semblance. This enables a consistent evaluation of the image focusing across both the reflection-angle axis and the structural-dip axis and improves the interpretability of the results.

The starting point of my method is an ensemble of prestack images, $\mathbf{R}(\mathbf{x},\gamma,\rho)$; these images are functions of a spatial coordinate vector $\mathbf{x}=\{z,x\}$ (with z depth and x the horizontal location), the aperture angle γ, and a velocity parameter ρ. The parameter ρ is the ratio between the new migration velocity and the migration velocity used for the initial migration. The ensemble of prestack images is obtained by residual prestack migration in the angle domain (Biondi, 2010); the proposed method could be easily adapted to the case where $\mathbf{R}(\mathbf{x},\gamma,\rho)$ is computed using residual prestack Stolt migration (Sava, 2003), or any other method that can efficiently generate ensembles of prestack images dependent on a velocity parameter.

To measure coherency along the structural dip α, I first create the dip-decomposed prestack image $\mathbf{R}(\mathbf{x},\gamma,\alpha,\rho)$. The decomposition can be efficiently performed in the Fourier domain during the residual prestack migration, or it could be performed in the space domain by applying recursive filters (Fomel, 2002; Hale, 2007). Notice that the dip-decomposed images I use as input have different kinematic characteristics than the ones described in Reshef and Rüger (2008), Landa et al. (2008), and Reshef (2008). These authors obtain dip-decomposed images by not performing the implicit summation over dips that is part of angle-domain Kirchoff migration (Audebert et al., 2002), whereas I decompose the migrated images.

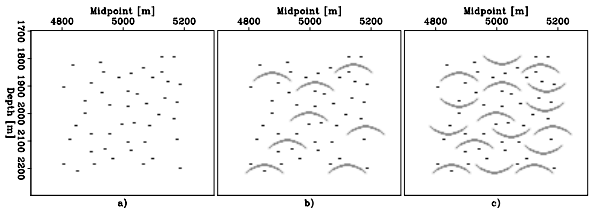

Figure 1: Reflectors geometry used to model the three zero-offset synthetic data sets I used to test the proposed image-focusing velocity-estimation method: (a) a "cloud" of point diffractors, (b) point diffractors and curved reflectors with positive curvature, (c) point diffractors, curved reflectors with positive curvature, and curved reflectors with negative curvature.

My first definition of the 2D image-focusing semblance is:

$$S_{(\gamma,\alpha)}(\mathbf{x},\rho)=\frac{\left[\sum_{\gamma}\sum_{\alpha}\mathbf{R}(\mathbf{x},\gamma,\alpha,\rho)\right]^2}{N_{\gamma}N_{\alpha}\sum_{\gamma}\sum_{\alpha}\mathbf{R}(\mathbf{x},\gamma,\alpha,\rho)^2}, \qquad (1)$$

where N_{γ} and N_{α} are, respectively, the number of aperture angles and the number of dips to be included in the computation. In the presence of point diffractors, the semblance functional defined in expression 1 yields unbiased estimates of the velocity parameter ρ. However, when the curvature is finite, the dip components would not be aligned for the correct value of ρ, and the estimates would be biased. To remove this bias, we can correct the dip-decomposed images for the presence of curvature by applying the spatial shift, $\Delta\mathbf{n}_{\text{Curv}}$, along the normal to the structural dip,

$$\Delta\mathbf{n}_{\text{Curv}}=\frac{\sin(\alpha-\bar{\alpha})\tan(\alpha-\bar{\alpha})}{2}R\mathbf{n}, \qquad (2)$$

where $\bar{\alpha}$ is the local dip, $\mathbf{n}$ is the vector normal to the dip α and directed towards increasing depth, and R is the local radius of curvature (Biondi, 2010). Notice that the application of correction 2 requires the estimation of local dip $\bar{\alpha}$. To estimate the local dips, I used a variant of the algorithms described by Fomel (2002).

Expression 2 can be used directly to create an ensemble of dip-decomposed images that are corrected for the local curvature $\mathbf{R}_{\text{Curv}}(\mathbf{x},\gamma,\alpha,\rho,R)$. The image-focusing semblance can be computed on these images as follows:

$$S_{(\gamma,\alpha)}(\mathbf{x},\rho,R)=\frac{\left[\sum_{\gamma}\sum_{\alpha}\mathbf{R}_{\text{Curv}}(\mathbf{x},\gamma,\alpha,\rho,R)\right]^2}{N_{\gamma}N_{\alpha}\sum_{\gamma}\sum_{\alpha}\mathbf{R}_{\text{Curv}}(\mathbf{x},\gamma,\alpha,\rho,R)^2}. \qquad (3)$$

The application of correction 2 to prestack data can be quite expensive. However, it can be efficiently performed together with residual migration (Biondi, 2010).

VELOCITY ESTIMATION FROM ZERO-OFFSET DATA: SYNTHETIC-DATA EXAMPLES

In this section, I present the application of the image-focusing semblance to the estimation of migration velocity from three zero-offset synthetic data sets. These data sets were modeled assuming reflectivity models of increasing complexity. The range of reflector curvature progressively increases from the first model to the third model.

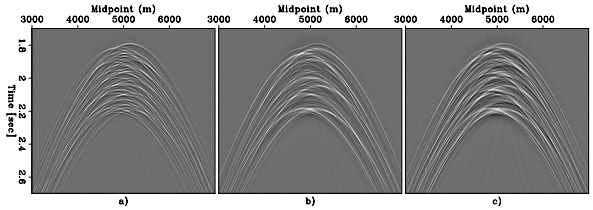

Figure 2: Zero-offset data modeled from the reflectivity functions shown in Figure 1.

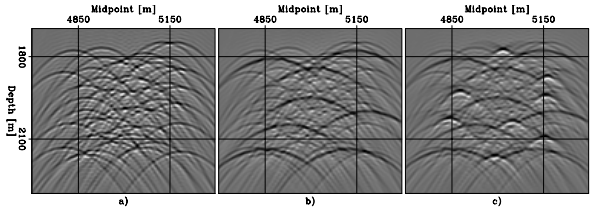

Figure 3: Migrated sections obtained by migrating the data shown in 2 with the initial (too low) velocity of 1.950 km/s. The inner squares delimited by the grid superimposed onto the images show the analysis windows, where the semblance is spatially averaged to produce the results shown in Figure 4.

Figure 1 shows the reflector geometry used to model the three synthetic data sets. I modeled the first data set assuming a "cloud"of 46 point diffractors (panel a). For the second data set, I added eight curved reflectors with positive radius of curvature of approximately 55 m (panel b). Finally, for the third data set, I added eight additional curved reflectors with a negative radius of curvature of approximately 55 m (panel c). I set the maximum amplitude of the curved reflectors to be about 40% of the maximum amplitude of the point diffractors to maintain a balance between the velocity information provided by the point diffractors and that provided by the curved reflectors. All the figures in this section follow the same pattern established in Figure 1. The left panels correspond to the reflectivity model shown in Figure 1a, the middle panels correspond to the reflectivity model shown in Figure 1b, and the right panels correspond to the reflectivity model shown in Figure 1c.

Figure 2 shows the three data sets modeled from the reflectivity models shown in Figure 1, assuming constant velocity equal to 2 km/s. The data increases in complexity and the texture changes as the curved reflectors are added to the reflectivity model.

Figure 3 shows the migrated sections obtained with the initial (too low) velocity of 1.951 km/s. The crossing of events in these images clearly indicates undermigration. The events corresponding to the reflectors with negative curvature are sufficiently undermigrated that they appear as reflectors with high positive curvature.

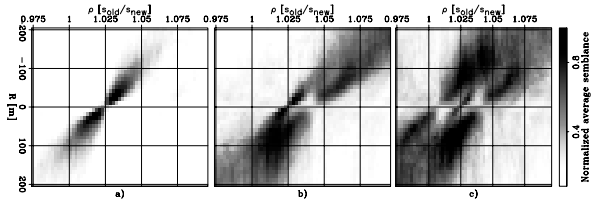

Figure 4: The image-focusing semblance spatially averaged over the analysis windows shown as a function of velocity parameter ρ and the radius of curvature R. Panel (a) shows the result corresponding to the point diffractors, panel (b) shows the result corresponding to the point diffractors and curved reflectors with positive curvature, and panel (c) shows the result corresponding to point diffractors, curved reflectors with positive curvature, and curved reflectors with negative curvature.

Figure 4 shows the results of the focusing analysis on the residual migrated ensembles obtained from the undermigrated images shown in Figure 3. All three panels show the image-focusing semblance spatially averaged in analysis windows defined by the following inequalities along the depth axis: 1.8 km $\leq$ z $\leq$ 2.1 km, and by the following inequalities along the midpoint axis: 4.85 km $\leq$ x $\leq$ 5.15 km. These analysis windows are represented in Figure 3 by the inner squares delimited by the grid superimposed onto the images. The panels show the average semblance as a function of the velocity parameter ρ and the radius of curvature R. The local dip $\bar{\alpha}$ used for the curvature correction (equation 2) was numerically estimated using a variant of the algorithms described by Fomel (2002).

The semblance panels show diagonal trends for all cases because of the velocity/curvature ambiguity. When only point diffractors are present, only one trend is visible and the pattern is symmetric around ρ=1.025; that is, the correct value of the parameter. The addition of the positive-curvature reflectors adds another trend to the semblance panel (Figure 4b) and breaks the symmetry. When reflectors with both negative and positive curvature are present (Figure 4c), the semblance maxima occur around the correct value (ρ=1.025) for all the trends in the panel.

In poorly focused images corresponding to ρ values both lower and higher than the correct one, the increase in range of reflector curvatures causes additional crossing events. These crossing events interfere with the local dip estimation and consequently with the curvature correction. As a result, the image-focusing semblance that measures dip coherency after the curvature correction is strongly attenuated for poorly focused images; only well-focused images correspond to high semblance values. To be statistically reliable, I average over a spatial window the velocity measures extracted from the data with this method. Therefore, I sacrifice spatial resolution for reduced velocity errors.

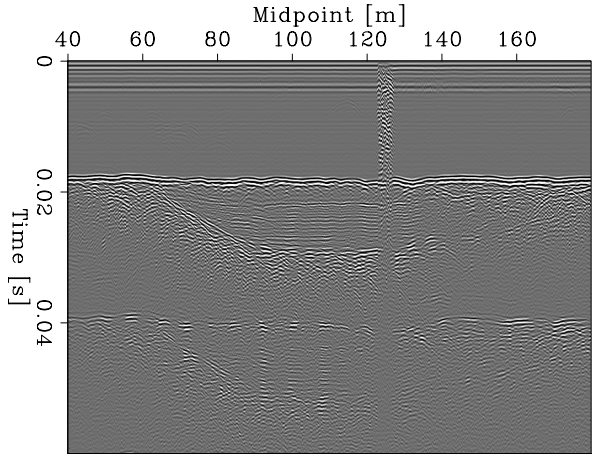

Figure 5: Zero-offset data recorded in New York Harbor using a 512i sub-bottom profiler with a 1-10 kHz pulse.

VELOCITY ESTIMATION FROM ZERO-OFFSET FIELD DATA

I tested the method for extracting velocity information from zero-offset data on a shallow seismic data set acquired in New York Harbor using a 512i sub-bottom profiler with a 1-10 kHz pulse. Figure 5 shows the subset of the data that I worked with. The water bottom primary reflection is recorded at about 18 milliseconds; strong multiple reflections are visible below the primaries. From nearby well-boring, the layered body in the middle is thought to be composed by Holocene sediments, mostly sands, with a velocity of approximately 2.150 km/s. The sediments are surrounded by serpentinite that has much higher seismic velocity. The serpentinite velocity ranges from 2.500 km/s where the rock is fractured (on the left of the sediments) to 4.300 km/s, where the rock is intact (below the sediments). I first migrated the data assuming a constant velocity equal to the velocity of water; that is, 1.500 km/s. Figure 6 shows the depth-migrated section.

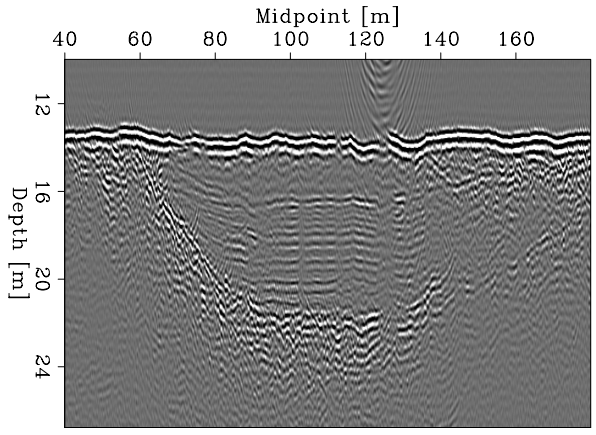

Figure 6: Depth-migrated section obtained assuming water velocity.

Image-focusing analysis

I performed the image-focusing analysis on a small analysis window; this window was centered on the events at flattish sediment-serpentinite interface at the bottom of the sediment layers. The depth of the analysis window ranged from 21 to 25 m, for the first iteration. I adjusted the depth for the following iterations to ensure that the analysis windows consistently included the same reflectors across iterations. Figure 7 shows the image-focusing semblance for the three iterations of the process as a function of the velocity parameter ρ and the radius of curvature R. To update interval velocity in the sediments from the picked ρ value, I followed conventional migration velocity analysis procedure for vertical velocity updating (Biondi, 2006). After the first iteration the updated velocity was $\widehat{V}_s$=2.250 km/s, and after the second, and final, update the velocity was $\widehat{V}_s$=2.155 km/s. The third iteration did not produce any update because the semblance peak in Figure 7c occurs at ρ=1, indicating that the process has converged.

Figure 8a and Figure 8b compare the entire image obtained with the initial velocity (top panel) with the entire image obtained with the final velocity (bottom panel). The improvements in the image are substantial outside the analysis window, as well as inside it. Outside the analysis window, the improvements are most noticeable in the areas indicated by the ellipses superimposed onto the sections. Figure 9a shows the analysis window for the initial image, and Figure 9b shows the analysis window for the final image. Compared with the first analysis window, the final analysis window shows substantial improvement in the continuity of the reflectors and a reduction in the number of crossing events.

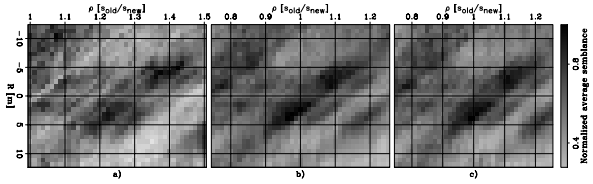

Figure 7: Image-focusing semblance computed from the migrated sections and spatially averaged over the analysis window: (a) first iteration, (b) second iteration, and (c) third iteration.

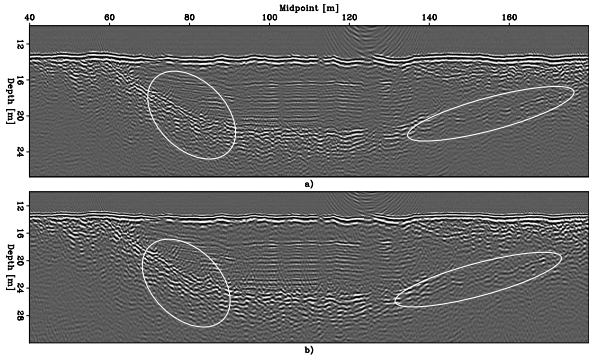

Figure 8: Whole image comparison: (a) initial image, (b) final image.

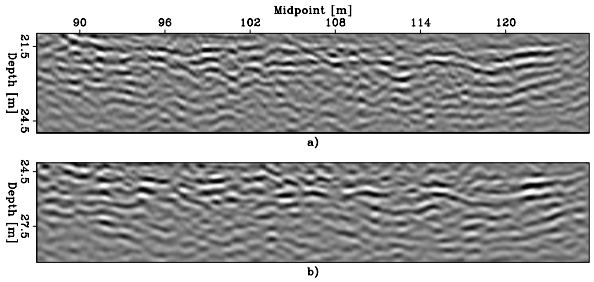

Figure 9: Analysis window comparison: (a) analysis window in the initial image, and (b) analysis window in the final image.

CONCLUSIONS

Using image focusing and unfocusing for velocity estimation has long been an elusive goal in reflection seismology. The main challenge is the ambiguity between image focusing and reflector curvature. Consequently, previously published methods rely on strong assumptions about reflector curvature, such as assuming that reflections were generated by point diffractors (i.e. infinite-curvature reflectors). I present a method that does not rely on this assumption, but instead it explicitly takes into account of reflector curvature when measuring image focusing. The image-focusing information that the proposed method extracts from prestack data is consistent with the velocity information that we routinely extract by measuring image coherency along the aperture-angle axes. Furthermore, because I compute semblance as a function of reflector curvature, the results are devoid of hidden bias toward high-curvature reflectors.

Velocity information can be successfully extracted from zero-offset data by analyzing the focusing and defocusing of residual-migrated images. The New York Harbor example demonstrate that the proposed method is sufficiently robust to provide reliable and quantitative velocity information from field data. The estimated interval velocity function is consistent with available geologic information and improves the focusing of the image both in the analysis window and outside the analysis window. The estimation method provides quantitative information on velocity without relying on subjective interpretive criteria. However, to achieve statistical stability, the semblance functional must be averaged over spatial windows, and thus spatial resolution is reduced.

ACKNOWLEDGMENTS

I thank the United States Army Corps of Engineers (USACE) New York District and Earthworks under contract number W912DS-06-D-0001 for providing the New York Harbor field data. I also would like to thank Daniel Rosales with Earthworks for his enthusiastic help in providing the data to the Stanford Exploration Project (SEP).

This research was conducted with the financial support of SEP's sponsors.

EDITED REFERENCES

Note: This reference list is a copy-edited version of the reference list submitted by the author. Reference lists for the 2010 SEG Technical Program Expanded Abstracts have been copy edited so that references provided with the online metadata for each paper will achieve a high degree of linking to cited sources that appear on the Web.

REFERENCES

Audebert, F., P. Froidevaux, H. Rakotoarisoa, and J. Svay-Lucas, 2002, Insights into migration in the angle domain: SEG Technical Program Expanded Abstracts, **21**, no. 1, 1188–1191, doi:10.1190/1.1816863.

Biondi, B., 2006, 3D Seismic Imaging: SEG.

Biondi, B., 2010, Velocity estimation by image focusing analysis: Geophysics, manuscript submitted for publication.

De Vries, D., and A. J. Berkhout, 1984, Velocity analysis based on minimum entropy: Geophysics, **49**, 2132–2142, doi:10.1190/1.1441629.

Fomel, S., 2002, Applications of plane-wave destruction filters: Geophysics, **67**, 1946–1960, doi:10.1190/1.1527095.

Fomel, S., E. Landa, and M. T. Taner, 2007, Poststack velocity analysis by separation and imaging of seismic diffractions: Geophysics, **72**, no. 6, U89–U94, doi:10.1190/1.2781533.

Hale, D., 2007, Local dip filtering with directional laplacians: CWP-Report, 567.

Harlan, W. S., J. F. Claerbout, and F. Rocca, 1984, Signal/noise separation and velocity estimation: Geophysics, **49**, 1869–1880, doi:10.1190/1.1441600.

Landa, E., S. Fomel, and M. Reshef, 2008, Separation, imaging, and velocity analysis of seismic diffractions using migrated dip-angle gathers: SEG Technical Program Expanded Abstracts, **27**, no. 1, 2176–2180, doi:10.1190/1.3059318.

Reshef, M., 2008, Interval velocity analysis in the dip-angle domain: Geophysics, **73**, no. 5, VE353–VE360, doi:10.1190/1.2957944.

Reshef, M., and A. Rüger, 2008, Influence of structural dip angles on interval velocity analysis: Geophysics, **73**, no. 4, U13–U18, doi:10.1190/1.2918741.

Sava, P., 2003, Prestack residual migration in the frequency domain: Geophysics, **68**, 634–640, doi:10.1190/1.1567233.

Sava, P. C., B. Biondi, and J. Etgen, 2005, Wave-equation migration velocity analysis by focusing diffractions and reflections: Geophysics, **70**, no. 3, U19–U27, doi:10.1190/1.1925749.

Stinson, K., E. Crase, W.-K. Chan, and S. Levy, 2005, Optimized determination of migration velocities: Recorder, **30**, 5–6.

Wang, B., V. Dirks, P. Guillaume, F. Audebert, and D. Epili, 2006, A 3D subsalt tomography based on wave-equation migration-perturbation scans: Geophysics, **71**, no. 2, E1–E6, doi:10.1190/1.2187720.